Hindawi
Mathematical Problems in Engineering
Volume 2022, Article ID 5370630, 11 pages
https://doi.org/10.1155/2022/5370630

Research Article

Multi-Source Data High-Performance Indoor Positioning considering Genetic Optimization Neural Network Algorithm

Peng Chu,[1] **He Zhang**,[2] **Yarong Chen**,[2] **Rui Zhu**,[2] **and Feng Wang**[2]

[1]*School of Mechanical Engineering, Xijing University, Xi'an, Shaanxi, China*
[2]*School of Information Engineering, Xijing University, Xi'an, Shaanxi, China*

Correspondence should be addressed to Peng Chu; 20170080@xijing.edu.cn

Received 12 April 2022; Accepted 25 June 2022; Published 21 July 2022

Academic Editor: Sagheer Abbas

In order to effectively solve the problem of relatively large errors in individual positioning strategies in indoor environments, this paper applies the genetic optimization neural network algorithm to indoor location based on multi-source information fusion. The range of the geomagnetic fitness is constrained based on the results obtained by using the wireless WiFi positioning for combination and matching, which can reduce the value of the matching error effectively. Subsequently, the global optimal value of the indoor network is calculated based on the genetic algorithm, which can optimize the initial value and threshold of the neural network after genetic optimization so as to improve the accuracy of the network to the greatest extent possible while accelerating the convergence speed at the same time. After the optimization processing is completed, fusion training can be performed on the coordinates of the actual positions based on the obtained combination positioning situation and the predicted positioning result in the indoor network. Finally, the optimal positioning result can be obtained accordingly. Through the analysis of practical cases, it can be known that the mean square error predicted based on the genetic optimization neural network calculated by using the genetic algorithm can be effectively reduced by 76%, and the accuracy of the fusion positioning can be increased by 48% on average compared with the accuracy of a single positioning strategy. Hence, the method put forward in this paper has effectively improved the positioning accuracy, which suggests that its positioning performance is superior.

1. Introduction

Due to the rapid advancement of wireless communication technology and multi-source data, multi-source data have been expensively applied in various fields as an emerging network technology. With regard to the flow of indoor multi-source data, in the high-performance scientific computing of daily multi-source data, the monitoring of real-time information of multi-source data has become more and more important in the multi-source data high-performance scientific computing industry [1–3]. Through setting up positioning and real-time monitoring on multi-source data high-performance scientific computing in real time, various data information in multi-source data high-performance scientific computing can be perceived [4–6]. Multiple sensor terminals can be used to implement monitoring and management. In this way, real-time monitoring and management can be implemented based on high-performance scientific computing. Due to the characteristics of high mobility and extensive network scale at the nodes corresponding to indoor flow distributed, higher reliability, stability, and security are required for real-time positioning and monitoring systems. The real-time positioning and monitoring system based on neural network computation with genetic optimization can analyze the multi-source data extracted and conduct high-performance scientific studies on this basis as compared to conventional methods. Hence, the equipment structure can be designed to be simpler, the cost is lower, and the maintenance is convenient, which has gradually become the trend of the

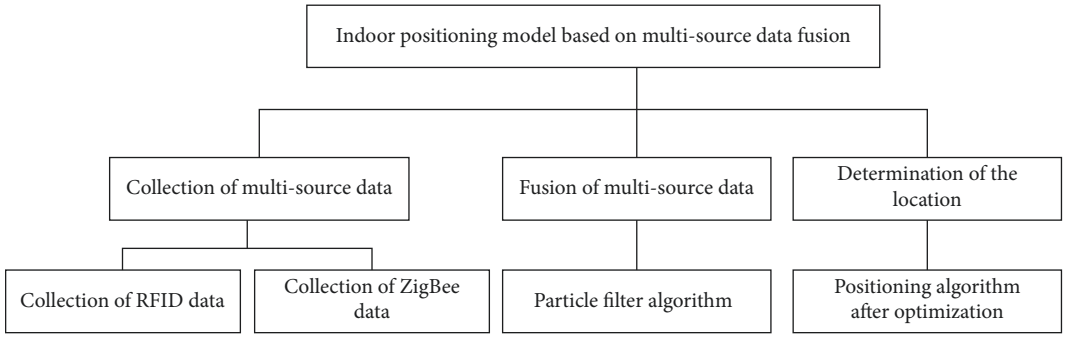

Figure 1: Architecture of the indoor location model based on multi-source data fusion.

continuous development of intelligent indoor real-time positioning and real-time monitoring systems.

In this paper, a multi-source data fusion indoor location model that effectively combines radio frequency and wireless WiFi technology is put forward based on the genetic optimization neural network algorithm. In addition, this technology is used to improve the positioning accuracy of unknown nodes by assigning different weights to various positioning nodes. Finally, the experimental results indicate that the algorithm proposed in this paper can fuse multi-source data and improve the performance of the positioning system effectively.

2. Methods

2.1. Design and Construction of a Positioning Model. The indoor location model designed in this paper can be roughly divided into data acquisition function module, data processing module, and location accurate positioning module. The structure of indoor location model is shown in Figure 1. The data acquisition module is mainly used to fuse the data collected by the system WiFi and use the multi-source data processing and analysis module to analyze the processed RF data. Effectively combine multi-source data fusion and neural network algorithm to complete the effective analysis of different types of data, collect different types of data, realize the high-performance scientific calculation of multi-source data, and improve the accuracy of indoor location.

From Figure 2, it can be observed that the indoor location based on high-performance scientific computing of multi-source data system is mainly composed of nodes, observation nodes, gateway, and host computer in the hardware module. The diagram of the corresponding system architecture is shown in Figure 3. In the system designed in this paper, the observation points can be roughly divided into RF reading function and wireless WiFi function module. The RF reading module can realize the accurate collection of RSSI data information. The wireless WiFi function module can process the obtained data information and send the processed data information to the gateway system as its own reference point. The selection of reference point is mainly based on the WiFi function module. Through the comparison and analysis with the observation point, from the perspective of organizational structure analysis, it can be seen that it can be widely used in many fields. The indoor location points can be integrated into RF tags, and the genetic neural network can be optimized and used in indoor location, which can effectively complete the accurate positioning of indoor points. Figure 3 shows the structure frame diagram of RF/wireless WiFi positioning system designed in this paper [7–9].

The accurate evaluation of indoor location shall be carried out according to the following seven calculation steps:

Step 1. According to the spatial structure layout of the indoor environment, the processed data are stored through the system coordinates corresponding to the observation point and reference point, the MAC address of the communication equipment, and the actual distance between adjacent nodes, and the assigned weight can be obtained from the perspective of node type w_{OP} and the weights of observation nodes w_{RP}.

Step 2. In indoor location based on the acquisition of node location, the related data on reference nodes are acquired and transmitted to the communication device in the upper layer, including the coordinates for three key nodes for indoor location. For the purpose of making wireless WiFi signals stronger and multi-source data computing more accurate, reference nodes corresponding to RF signals are adopted. Through valid combination, the data acquired by the system can be filtered by the particle filter algorithm.

Step 3. Based on the intensity of RF and wireless WiFi signals corresponding to the above reference nodes for indoor location, the practical distance between unknown and known nodes is

$$\text{RSSI}\,(d) = A - 10n\lg d, \tag{1}$$

where A represents the intensity of signals at 1 m and n represents the loss coefficient at the corresponding node.

Step 4. The reference node is taken as the center of the circle, and the corresponding recognition distance is taken as the radius. The reference node recognition is shown in Figure 4. According to equation (2), the intersection point (x_{bc1}, y_{bc1}), (x_{bc2}, y_{bc2}) between circle B and circle C, the intersection point (x_{ac1}, y_{ac1}), (x_{ac2}, y_{ac2}) between circle A and circle C,

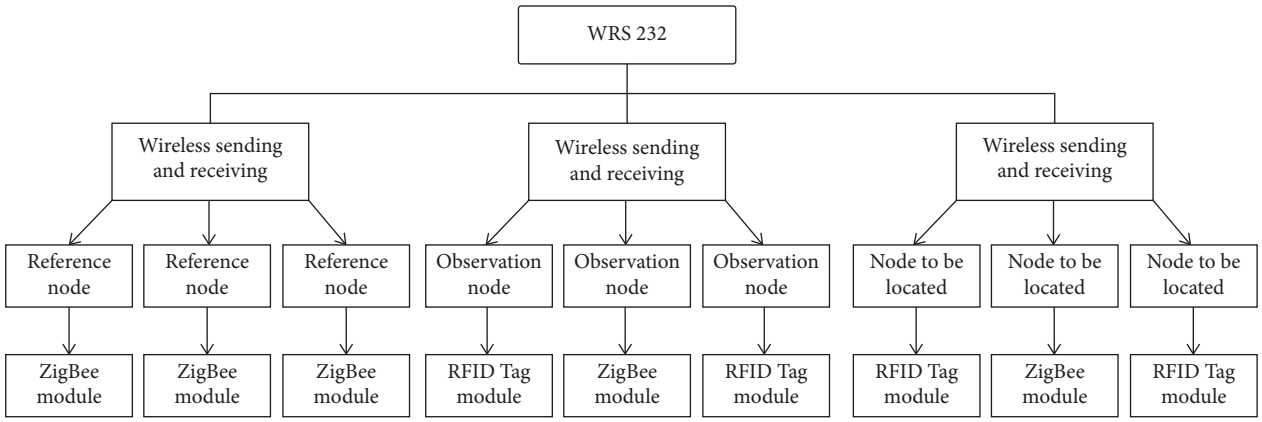

Figure 2: Hardware block diagram of the positioning model.

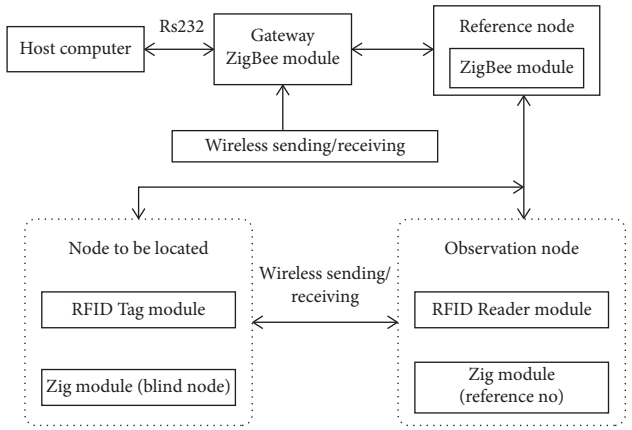

Figure 3: Block diagram of radio frequency/wireless WiFi fusion positioning system.

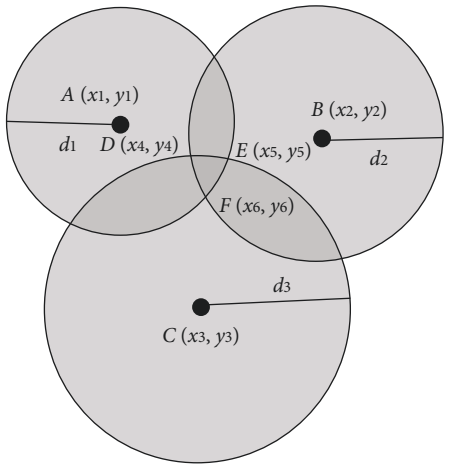

Figure 4: Diagram of the positioning algorithm.

and the intersection point (x_{ab1}, y_{ab1}), (x_{ab2}, y_{ab2}) between circle A and circle B can be obtained through calculation. The distance Eq. $(x - x_1)^2 + (y - y_1)^2$ corresponding to the intersection of B and C can be used to calculate the intersection $D(x_4, y_4)$ of the two intersections that are closer to A. Thus, it can be known that the distance B between points A and C is closer to the intersection $E(x_5, y_5)$, and the distance to C is closer to the intersection point $F(x_6, y_6)$.

$$d_i = \sqrt{(x - x_i)^2 + (y - y_i)^2}, \quad i = 1, 2, 3. \tag{2}$$

Step 5. According to the connection of a triangular shape composed of point D, point E, and point F designed in the positioning algorithm, the obtained RSSI values corresponding to node a, node B, and node C are divided into node D, node E, and node F. The detailed division of the three nodes is shown in Table 1.

$\text{RSSI}_{\max}(d)$ is defined by subtracting the RSSI of the node with the highest signal intensity from that of nodes with other signal intensity:

$$\left|\text{RSSI}_{\max}(d)\right| - \left|\text{RSSI}_i(d)\right| = A - 10n\lg d_i - A + 10n\lg d_{\max}, \quad i = 1, 2, 3,$$

$$w_i = \frac{d_{\max}}{d_i} = 10^{\dfrac{\left|RSSI_{\max}(d)\right| - \left|RSSI_i(d)\right|}{10n}}, \quad i = 1, 2, 3. \tag{3}$$

From the reference node, the coordinates (x, y) of unknown nodes are inferred according to equation (5):

$$(x, y) = \left(\frac{w_1 \cdot x_4 + w_2 \cdot x_5 + w_3 \cdot x_6}{w_1 + w_2 + w_3}, \frac{w_1 \cdot y_4 + w_2 \cdot y_5 + w_3 \cdot y_6}{w_1 + w_2 + w_3}\right). \tag{4}$$

Table 1: RSSI allocation table corresponding to three nodes.

Node 1	Node 2	Intersection point	Distribution point
A	E	A	D
C	F	E	A
D	C	C	A

The above algorithm is used to estimate the coordinates (x_{RP}, y_{RP}) of a specific node at a location.

Step 6. The relevant data of the surrounding observation nodes are collected at the location node again, and Step 3 to Step 5 are repeated to calculate the coordinate estimation value (x_{OP}, y_{OP}) of the location node.

Step 7. The final coordinates of the unknown node are calculated based on equation (6) as the following.

$$(x, y) = \left(\frac{x_{RP} \cdot w_{RP} + x_{OP} \cdot w_{OP}}{w_{RP} + w_{OP}}, \frac{y_{RP} \cdot w_{RP} + y_{OP} \cdot w_{OP}}{w_{RP} + w_{OP}} \right). \tag{5}$$

2.2. Principles of Indoor Location Technology. The advantages and disadvantages of the current single-source positioning technology are combined, as shown in Table 2. As single-source positioning technology has a certain number of restrictions, first of all, the wireless WiFi technology can meet the communication capabilities required by the radio frequency positioning technology. Secondly, radio frequency positioning technology can also be embedded into wireless WiFi positioning technology to improve and make up for the defect of low positioning accuracy.

The principle of indoor location based on high-performance scientific computing of multi-source data technology is described in Figure 5, in which E and N stand for the east and north of the position, respectively. It is assumed that the initial position is (x_0, y_0), when the pedestrian takes a step, the inertial sensor calculates the current heading θ and step length d in real time, and then solves the next position (x_1, y_1) according to the (1), and so on. Finally, the current position (x_i, y_i) of the pedestrian can be obtained.

$$\begin{bmatrix} X_i \\ Y_i \\ \theta_i \end{bmatrix} = \begin{bmatrix} X_{i-1} + d_i \cos\theta_i \\ Y_{i-1} + d_i \sin\theta_i \\ \theta_i \end{bmatrix}. \tag{6}$$

In the above equation, θ_i represents the heading angle of the ith step, X_{i-1} and Y_{i-1} stand for the coordinates of the i_1th step, and X_i and Y_i stand for the coordinates of the ith step.

As shown in equation (2), the most common model for the estimation step has relatively high accuracy, which is also conducive to the empirical relationship between the accelerometer mode value and the step length.

$$L = K\sqrt[4]{A_{\max} - A_{\min}}. \tag{7}$$

In the above equation, K is used to represent the calibration coefficient, $A_{\max}$ and $A_{\min}$ stand for the maximum and minimum acceleration of any step, respectively, and both values are obtained based on the gait discrimination conditions.

2.2.1. Acquisition and Filtering. Based on the expression 1 and expression 3, the distance between different types of ranging methods and fixed nodes can be calculated. However, when the data information is collected, different external interferences will be generated at the same time. The data obtained after multiple measurements are not correlated. Hence, compared with the moving average algorithm, the algorithm adopted in this paper can make up for the defect of high storage space requirements based on the moving average algorithm and optimize the distance measurement value by combining the linear combination of historical data. The expression is shown as the following:

$$\begin{aligned} \overline{d}_{n+1} &= \frac{1}{k+1} \sum_{i=n-k+1}^{n+1} d_i = \frac{1}{k+1} \left(d_{n+1} + k\overline{d}_n \right), \\ &= \frac{1}{k+1} d_{n+1} + \frac{k}{k+1} \overline{d}_n. \end{aligned} \tag{8}$$

The previous moment can be expressed as the following:

$$\overline{d}_k = (1 - \beta) d_n + \beta \cdot \overline{d}_{n-1}. \tag{9}$$

If $\beta = k/k+1$ is met and $0 \le \beta < 1$, the corresponding exponential weighting factor β is used as the weight of the latest data. It is assumed that the value of β gets larger, the impact on the data will be smaller and vice versa. Based on the above equation, $\overline{d_R}$ and $\overline{d_T}$ can be obtained as the following.

$$\widehat{d}_R(n) = \begin{cases} \widehat{d}_R(n-1) + v_{\max} T, & \overline{d}_R(n) - \widehat{d}_R(n-1) \ge v_{\max} T, \\ \widehat{d}_R(n-1) - v_{\max} T, & \overline{d}_R(n) - \widehat{d}_R(n-1) \le -v_{\max} T, \\ \overline{d}_R(n), & \text{others}, \end{cases}$$

$$\widehat{d}_T(n) = \begin{cases} \widehat{d}_T(n-1) + v_{\max} T, & \overline{d}_T(n) - \widehat{d}_T(n-1) \ge v_{\max} T, \\ \widehat{d}_T(n-1) - v_{\max} T, & \overline{d}_T(n) - \widehat{d}_T(n-1) \le -v_{\max} T, \\ \overline{d}_T(n) & \text{others}. \end{cases} \tag{10}$$

2.2.2. Genetic Optimization. Based on the application of wireless communication, the two wireless nodes can be set to a visible environment [10–12]. In this case, a system state model based on the kinematics principle is established in this paper as the following:

$$\begin{cases} \dot{s}(t) = v(t), \\ d(t) = s(t). \end{cases} \tag{11}$$

Thus, the above model can be discretized as the following:

Table 2: Comparison of the performance of indoor location technologies.

Positioning technology	Accuracy	Penetrability	Anti-interference	Cost
Ultrasound	Very high	Low	Moderate	Very high
Infrared	Relatively high	Very low	Very low	Relatively low
Radio frequency	Very high	Moderate	Relatively low	Relatively low
Wireless WiFi	Relatively low	Relatively high	Moderate	Moderate
Bluetooth	Moderate	Moderate	Relatively low	Moderate
WiFi	Low	Moderate	Very high	Low
Ultra-wideband	Very high	Very high	Relatively high	Relatively high

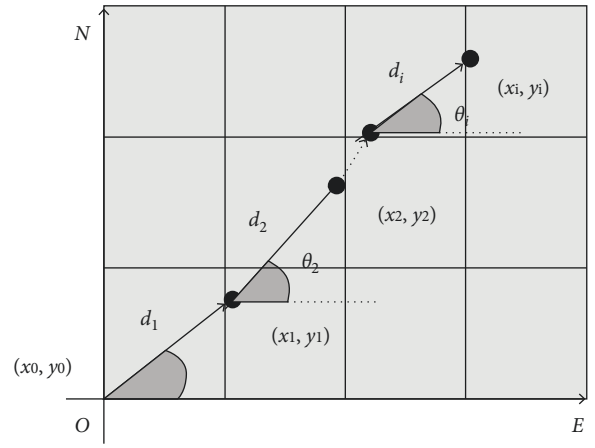

Figure 5: Schematic diagram of the indoor location technology based on high-performance scientific computing of multi-source data.

$$\begin{cases} s(n+1) = s(n) + T \cdot v(n) + T \cdot \xi(n), \\ d(n) = s(n) + \eta(n). \end{cases} \tag{12}$$

In the above equation, the variables $s(n)$ and $v(n)$ stand for the distance and radial velocity of n nodes received by this node, respectively; T represents the sampling period. However, based on the linear system with unknown noise distribution, genetic optimization algorithm is the most preferred method for state estimation. Through equation (12), the KF prediction equation can be obtained as the following:

$$\begin{cases} \hat{s}^*(n+1) = \hat{s}(n) + T \cdot \hat{v}(n), \\ \hat{d}^*(n+1) = \hat{s}^*(n+1), \\ \sigma_s^{*2}(n+1) = \sigma_s^2(n) + T^2 \sigma_\xi^2(n). \end{cases} \tag{13}$$

The $\sigma_s^2(n)$ and $\sigma_\xi^2(n)$ in the above equation stand for the nth ACK data that the node can receive, respectively, which are mainly the degrees of changes in $\hat{r}(n)$ and $\zeta(n)$. At this point, the updated equation can be obtained as the following:

$$\begin{cases} K(n+1) = \sigma_s^{*2}(n+1)\left[\sigma_s^{*2}(n+1) + n_\eta^2(n+1)\right]^{-1}, \\ \hat{s}(n+1) = \hat{s}^*(n+1) + K(n+1)\left[\hat{d}(n+1) - \hat{d}^*(n+1)\right], \\ \sigma_s^2(n+1) = \left[1 - \sigma_s^{*2}(n+1)\right]K(n+1). \end{cases} \tag{14}$$

In the above equation, $K(n+1)$ represents the genetic optimization gain and $\sigma_\eta^2(n+1)$ represents the amount of changes in the noise $\sigma_\eta(n+1)$ when the node receives the $(n+1)$th data packet. In practical applications, different distribution estimates can be made for $\eta(n)$ based on the different environments where $\sigma_\eta^2(n)$ is located.

2.3. WiFi/Geomagnetic Combination Positioning Method

2.3.1. Establishment of a Multi-Source Database

(1) WiFi Data. Based on the collection method, the location determination scene is divided into n grids with a size of 0.6 m $*$ 0.6 m. For each grid, more than 110 sets of WiFi intensity data are collected for multiple APs (wireless access points) configured, and the mean values are calculated to form a multi-source data sequence group accordingly. Taking the instability of the WiFi signal into consideration, the difference between the selected WiFi signal intensities of the measured point signal intensity should be below a certain threshold value, as shown in equation (15).

$$\left|R_i - M_i\right| \le S_{th}\,(i = 1, 2, \ldots, n). \tag{15}$$

In the above equation, M_i indicates that the WiFi signal intensity can be optimized for i grid nodes; R_i indicates that the WiFi signal intensity corresponding to the ith grid node can be obtained based on the measured intensity data of 15 nonabnormal WiFi signals; S_{th} represents the intensity threshold; and 5 dBm is taken as its value in this paper in order to guarantee the accuracy of data collected.

Figure 6 shows a group of WiFi multi-source data, and the mean value of the actual WiFi signal intensity is −46.33 dBm. Under the constraint conditions, the data point at the arrow is detected and deleted as a point far away from the cluster, which can also effectively improve the accuracy of WiFi multi-source data.

The WiFi multi-source data on the ith grid node are expressed in the equation as the following.

$$FW_i = \{pos_i, RSS_i\}\,(i = 1, 2, \ldots, n). \tag{16}$$

In the above equation, pos_i represents the real coordinates of the ith grid node and RSS_i represents the WiFi multi-source data sequence preprocessed by the ith grid node.

(2) Geomagnetic Data. The magnetic multi-source data are collected by using a magnetometer. However, as the

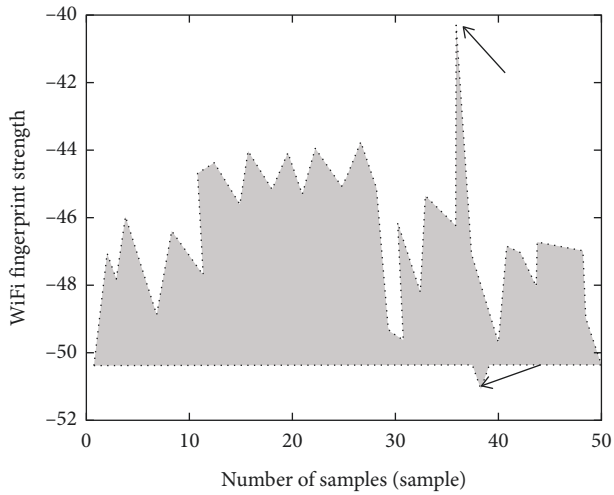

Figure 6: Detection of outliers in the WiFi multi-source data.

magnetometer will inevitably have errors due to the production technology, it is necessary to carry out compensation and correct the errors present.

From Figure 7, it can be observed that the center of the sphere formed by the magnetometer data is not at the origin of the coordinates. The reason is due to the zero deviation error of the magnetometer used, and the least square method is used in this paper to correct the error of the magnetometer. The three-dimensional distribution diagram of the compensated magnetometer data is shown in Figure 8, in which the center of the sphere is located at the origin of the coordinates.

2.3.2. Multi-Source Data Matching Algorithm. The multi-source data matching algorithm can accurately measure two multi-source data sequences with different lengths and effectively maintain the primary characteristics of the multi-source data sequence initially obtained, while ensuring a higher accuracy of the results thus obtained at the same time. Hence, multi-source data matching algorithm is used in this paper to match the data array.

If the sequence of the initial multi-source data is X, Y, and the length is $|X|$ and $|Y|$, then the following can be obtained after genetic optimization $w = \omega_1, \omega_2, \ldots, \omega_k$:

$$\max(|X|, |Y|) \le k \le |X| + |Y|. \tag{17}$$

In the above equation, k represents the final stretched length of the two sequences.

For the purpose of implementing genetic optimization, it is necessary to conduct at $\omega_1 = (1, 1)$ and end at $\omega_k = (|X|, |Y|)$ to ensure that the coordinate points corresponding to the X and Y sequences appear once each. Thus, the variables i and j in $\omega_k = (i, j)$ after genetic optimization can present a monotonic increase, and the corresponding monotonic increase is shown as the following:

$$\omega_k = (i, j), \quad \omega_{k+1} = (i', j'), \quad i \le i' \le i + 1, \quad j \le j' \le j + 1. \tag{18}$$

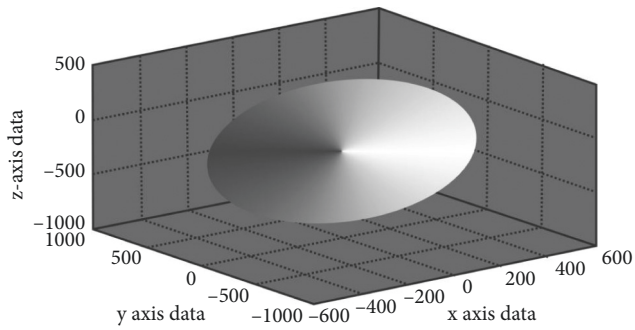

Figure 7: Three-dimensional distribution diagram of original signals of the magnetometer.

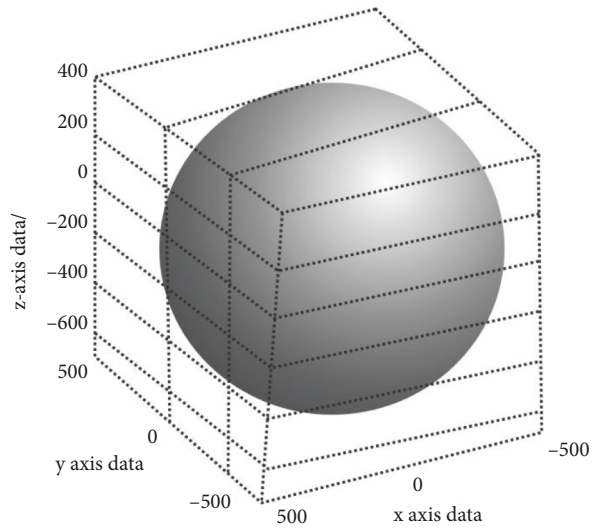

Figure 8: Three-dimensional distribution diagram of signals of the magnetometer after calibration.

Hence, the matrix $D(i, j)$ for genetic optimization can be obtained as the following:

$$D(i, j) = \mathrm{Dist}(i, j) + \min\{D(i-1, j), D(i, j-1), D(i-1, j-1)\}. \tag{19}$$

$D(i, j)$ represents the similarity between the first i points of the X sequence and the first j points of the Y sequence. The genetic optimization distance is $D(|X|, |Y|)$. If the value of $D(|X|, |Y|)$ gets smaller, the sequence similarity of the original multi-source data will be higher.

2.3.3. WiFi/Geomagnetic Combination Positioning Method. Combined with the WiFi and magnetic positioning characteristics, the geomagnetic positioning matching range is effectively limited based on the WiFi positioning error, but also significantly reduces the error rate of magnetic field matching [13–15]. Among them, Figure 9 shows the positioning process, using WiFi/geomagnetic coupling.

From Figure 9, it can be observed that the magnetic field matching range is limited to the center of the WiFi positioning result ($\mathrm{pos}_{\mathrm{WiFi}}$), and the WiFi positioning error is

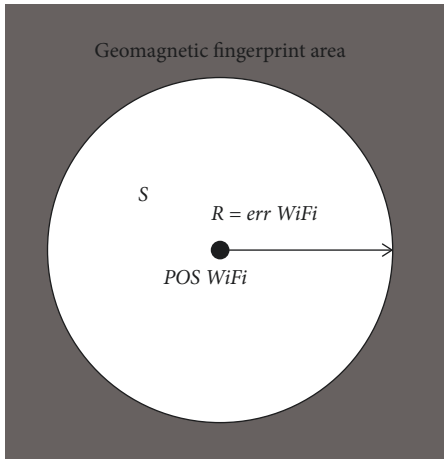

Figure 9: Schematic diagram of WiFi/geomagnetic combination positioning.

within the radius ($\mathrm{err}_{\mathrm{WiFi}}$) of the circular area S; that is, in the case of actual computation, it is consistent with the geomagnetic multi-source data within the circular area only, whereas the other multi-source data in the multi-source database are not included in the matching range. Finally, the result of combination positioning can be obtained.

$$\mathrm{COM}_{pos} = \mathrm{DTW}\{FM_i \in S\}\,(i = 1, 2, \ldots, n). \tag{20}$$

In the above equation, $\mathrm{COM}_{\mathrm{pos}}$ represents the result of the combination positioning, and $\mathrm{DTM}\{\mathrm{FM}_i \in S\}$ represents the matching of n magnetic field sequences FM in the area S based on the DTW algorithm.

In summary, the flowchart of the WiFi/geomagnetic combination positioning can be obtained, as shown in Figure 10.

2.4. Fusion Positioning Method of the Genetic Optimization Neural Network Algorithm. The results of indoor location based on high-performance scientific computing of the source data and the results of WiFi/geomagnetic coupling positioning are trained in the direction of the coordinates at the actual location to obtain the optimal fusion positioning results.

2.4.1. Design the Genetic Optimization Neural Network. (1) Establishment of the Model for the Genetic Optimization Neural Network.

Figure 11 shows the diagram of a typical three-layer neural network after genetic optimization.

The output is denoted as o_i, and the input to the middle layer by the jth node can be obtained:

$$\begin{aligned} \mathrm{net}_j &= \sum_j w_{ji} o_i, \\ o_j &= f\left(\mathrm{net}_j\right), \\ \mathrm{net}_k &= \sum_j w_{kj} o_j, \\ \widehat{y}_k &= o_k = f\left(\mathrm{net}_k\right). \end{aligned} \tag{21}$$

Network error refers to the difference between the expected and actual outputs, i.e., $e_k = y_k - \widehat{y}_k$.

$$E = \frac{1}{2} \sum_{n=1}^{i} \left(y_k - \widehat{y}_k\right)^2. \tag{22}$$

(2) Determine the Training Sample. With regard to the genetic optimization neural network, its target input is a 4D matrix including the results of indoor location based on high-performance scientific computing of multi-source data and WiFi/geomagnetic coupling. The final training sample is shown in

$$\begin{cases} \text{Input Data} = \begin{bmatrix} x_{pi} \\ y_{pi} \\ x_{ci} \\ y_{ci} \end{bmatrix} (i = 1, 2, \ldots, n), \\ \text{Target Data} = \begin{bmatrix} x_{ri} \\ y_{ri} \end{bmatrix}. \end{cases} \tag{23}$$

In the above equation, InputData represents the input sample, and (x_{pi}, y_{pi}) and (x_{ci}, y_{ci}) stand for the coordinates of the ith point to be positioned by using the indoor location based on the high-performance scientific computing of multi-source data and the coordinates obtained by using WiFi/geomagnetic combination positioning, respectively; TargetData represents the target output sample, and (x_{ri}, y_{ri}) represents the coordinates of the real position of the ith point to be positioned.

(3) Determine the Neuron Parameters. The number of neurons is determined and expressed by using the empirical equationas follows:

$$m = \sqrt{n + l} + a. \tag{24}$$

a represents a constant between 1 and 10.

2.4.2. Design of the Genetic Optimization Neural Network Algorithm. The main steps are described as the following.

(1) Determination of the coding method and initial population.

(2) Select the fitness function.

Based on the difference between the actual and expected network outputs, the adaptive function is generally determined, and the function for the matching degree is selected according to

$$E = \sum_{i=1}^{n} \left(T_i - Y_i\right)^2. \tag{25}$$

(3) Select the selection operator.

The ith individual will be retained as the following:

$$P_{si} = \frac{f_i}{\sum_{j=1}^{n} f_j}. \tag{26}$$

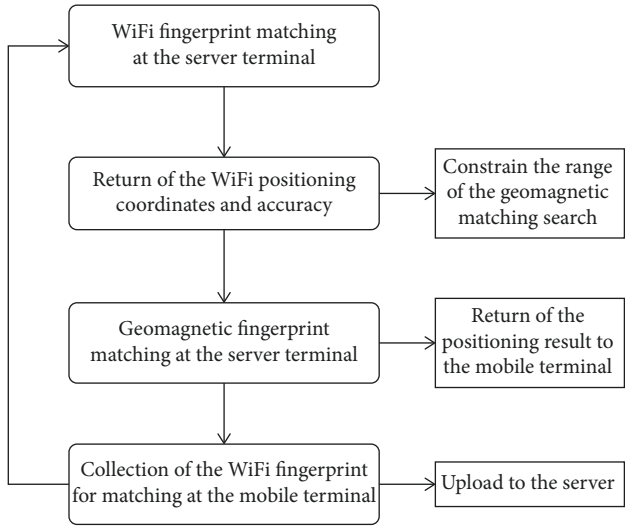

Figure 10: Flowchart of the WiFi/geomagnetic combination positioning.

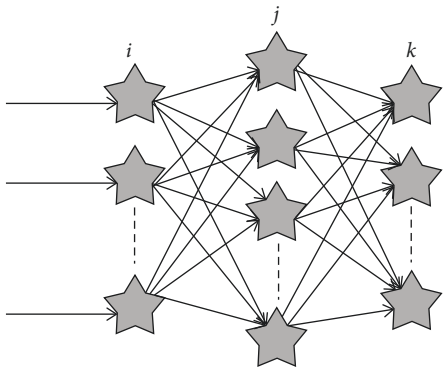

Figure 11: Architecture diagram of the genetic optimization neural network.

(4) Selection of crossover operator.

In this paper, the overall crossover scheme is selected, as shown in

$$\alpha = \begin{cases} \dfrac{f_{\max} - f_i}{f_{\max} - f_{avg}}, & f_i \geq f_{avg}, \\ 0.35, & f_i < f_{avg}. \end{cases} \tag{27}$$

In the above equation, α represents the gene encoding combination coefficient.

The process for the genetic optimization neural network finally obtained is shown in Figure 12.

3. Analysis of Experimental Results

3.1. Simulation Experiment of the Algorithm. In order to verify that the neural network performance is optimized after genetic algorithm optimization, this paper collects fusion simulation analysis based on WiFi/geomagnetic coupling positioning and indoor location X-axis coordinate data based on multi-source data high-performance scientific

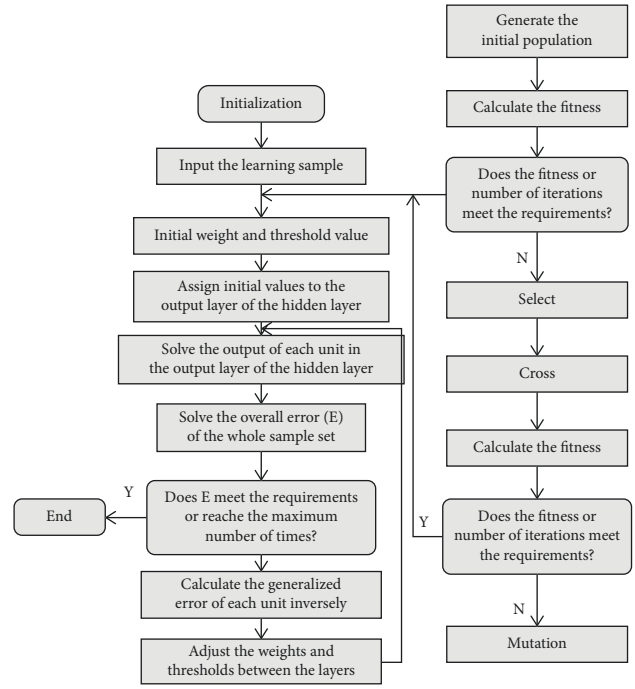

Figure 12: Flowchart of the genetic optimization neural network algorithm.

computing. The training sample collection scene is a 250-m-long straight-line area with a collection interval of 0.6 m. There are 900 samples in total, 700 samples are used for training, and 200 samples are used for testing. The input layer in the genetic optimization neural network structure has two nodes: the hidden layer has five nodes, and the output layer has one node. There are 15 weights and 6 thresholds. Hence, the personal password length of the genetic algorithm is 21.

3.1.1. Prediction Output and Error of the Genetic Optimization Neural Network without Optimization. The prediction output of the x-axis coordinates and the prediction error obtained based on the BP network fusion algorithm are shown in Figures 13 and 14, respectively.

3.1.2. Prediction Output and Error of the Genetic Optimization Neural Network after the Optimization of the Genetic Algorithm. Figure 15 shows the change in the optimal individual fitness value in the genetic algorithm optimization process.

Table 3 shows the optimal initial value and threshold value of the genetic optimization neural network obtained after the optimization of the genetic algorithm.

In the above table, $W1$ represents the weight between the input layer and the hidden layer, $B1$ represents the threshold value of the hidden layer node, $W2$ represents the weight between the hidden layer and the output layer, and $B2$ represents the threshold value of the output layer node.

The prediction output of the genetic optimization neural network optimized by the genetic algorithm is shown in

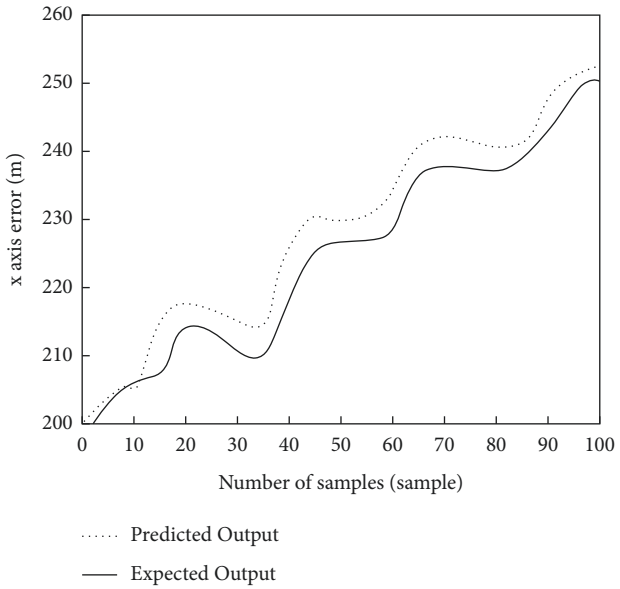

Figure 13: Prediction output of the genetic optimization neural network without optimization.

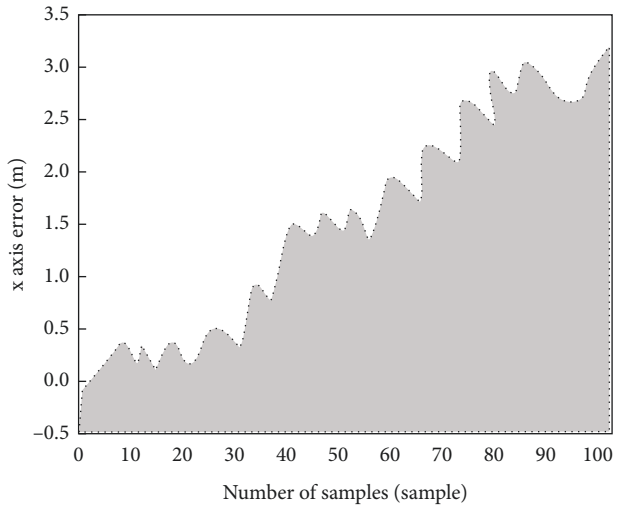

Figure 14: Prediction error of the genetic optimization neural network without optimization.

Figure 16, and the prediction error of the genetic optimization neural network optimized by the genetic algorithm is shown in Figure 17.

It can be observed from Figures 16 and 17 that the prediction result of the BP network is more accurate. The mean square error before the optimization is 0.447 meters, whereas the mean square error after the optimization is 1.7615 meters, and the mean square error is reduced by about 75%, which has verified the feasibility of the fusion algorithm.

3.2. Functional Experiment of Positioning. The corridor in the classroom building is selected as the experimental environment (14 m ∗ 20 m). The experimental field is divided into grids at a size of 1 m * 1 m, and motion is carried out for each detection (about 0.5 m). As shown in Figure 18, positioning is triggered for each motion.

Six APs are set up in the environment. The WiFi intensity and magnetic field intensity are collected using

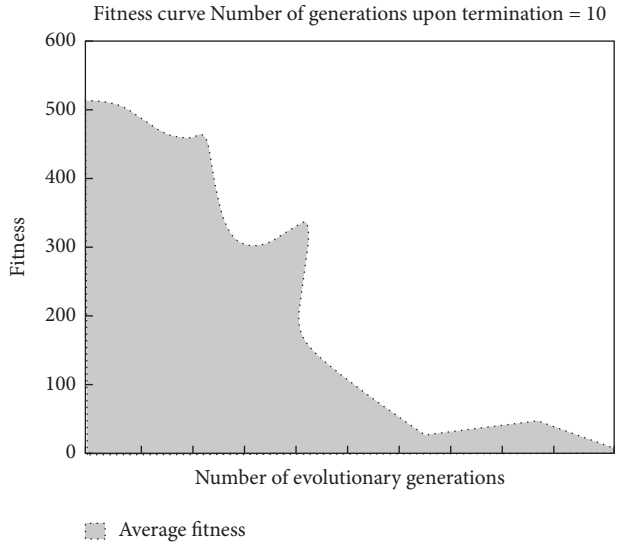

Figure 15: Adaptation curve.

Table 3: Initial value and threshold of the genetic optimization neural network after optimization.

Weight and threshold values	Parameter value				
$W1$	−0.723	1.067	2.964	1.665	−2.767
	2.357	0.268	1.183	−1.455	−0.078
$B1$	0.157	−2.878	−1.101	2.454	0.359
$W2$	2.255	1.557	1.700	2.667	2.937
$B2$	−1.334				

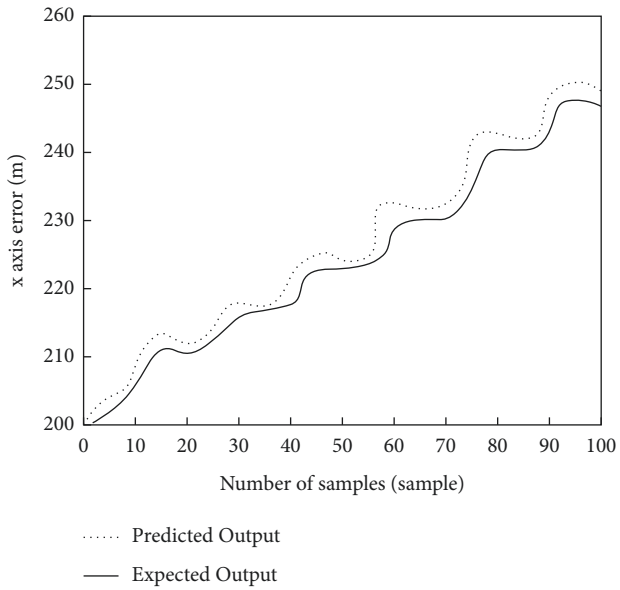

Figure 16: Predicted output of the genetic optimization neural network after optimization of the genetic algorithm.

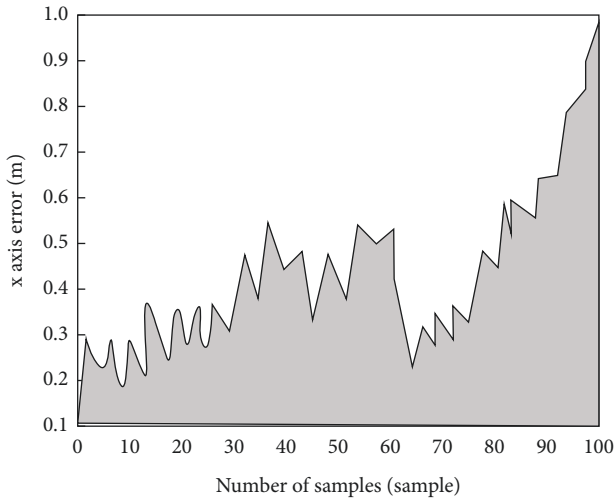

Figure 17: Prediction error of genetic optimization neural network after optimization of the genetic algorithm.

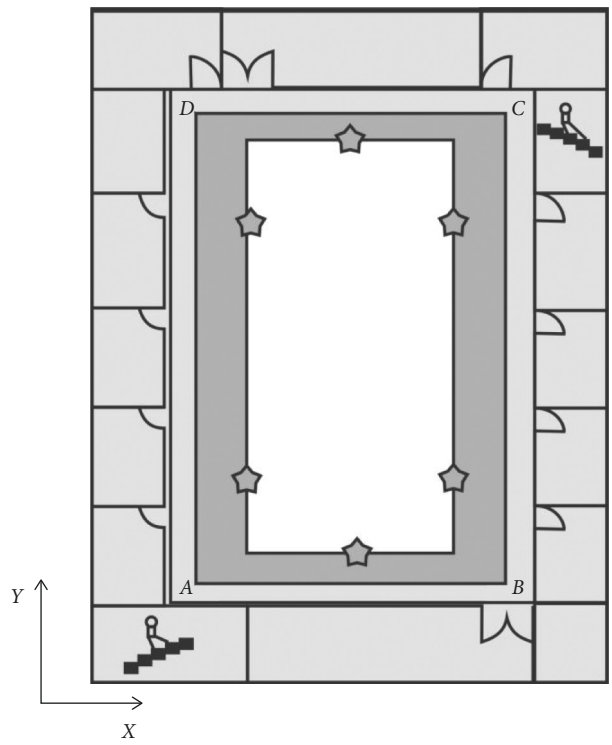

Figure 18: Layout plan of the experimental scene.

mobile phones and self-developed APP in real time. The experimental path is A-B-C-D-A.

3.2.1. Acquisition of the Positioning Data. In order to improve the real-time performance of positioning data acquisition, by establishing WiFi based on socket communication on the server side, the magnetic multi-source database can be saved in the database server, and the multi-source data positioning algorithm can also be used. Download to the server. In addition, MATLAB simulation

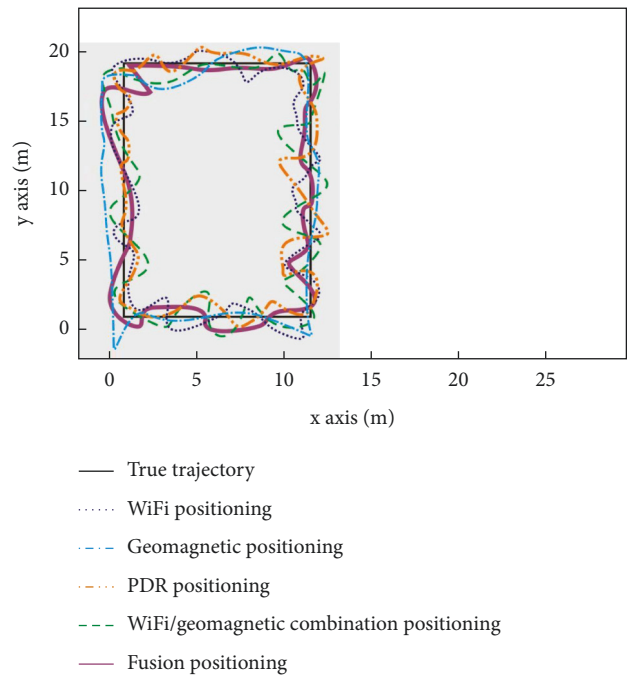

Figure 19: Positioning results based on different positioning methods.

software is used to simulate the indoor location construction based on multi-source data high-performance scientific computing. When the indoor location of high-performance scientific computing based on multi-source data is started, the system will send the collected data information, geomagnetic data, and sensor data to the server together. Finally, after the server receives the data information, it will locate according to the genetic optimization algorithm and feed the result back to the locator.

3.2.2. Analysis of the Positioning Accuracy. Figure 19 shows the reproduction results of the motion trajectories obtained based on different positioning methods. It can be known that the results obtained based on WiFi and geomagnetic positioning are prone to deviating from the actual coordinates. Although the coupled positioning has effectively improved the defects of two single positioning to some extent, there is still a range of error fluctuations. In the indoor location based on high-performance scientific computing of multi-source data in the 5 steps before departure, the positioning result is close to the real coordinates. Due to the influence of the cumulative error, the error of the coordinates when returning to the origin is relatively huge, whereas the positioning accuracy of neural network fusion after genetic improvement can be significantly improved.

Based on the different values of the positioning average errors obtained in Table 4, the accuracy of effectively obtaining combination positioning can be improved by about 17% compared with the positioning accuracy of using WiFi alone. Hence, the accuracy of the algorithm proposed in this paper is about 47% higher than that of the high-performance indoor location, with relatively good positioning performance.

Table 4: Comparison of the average positioning errors.

Method of positioning	WiFi positioning	Geomagnetic positioning	High-performance indoor location	WiFi/geomagnetic combination positioning	Positioning based on the algorithm scheme proposed in this paper
Average error (m)	0.544	0.644	1.2156	0.445	0.378

4. Conclusions

In view of the relatively huge error in the current indoor location based on a single method before the application of the genetic optimization neural network algorithm, the wireless WiFi, geomagnetism, and multi-source data are used in this paper to extract the coordinates based on indoor location, which are characterized by the fact that this function can be implemented with a mobile phone. In this way, the calculation can be simplified so that the algorithm can be implemented more effectively. The problem of slow convergence is solved effectively by using the genetic algorithm, and the method of network prediction average is adopted, which can reduce the workload by 76%. The accuracy of fusion positioning can be improved by 48% compared with that of the positioning method. Based on the method put forward in this paper, the sensors and WiFi hotspots built in the mobile terminal can be used; that is, in a continuous and stable indoor location situation, even if the wireless WiFi signal disappears, the continued positioning can still be carried out, which has demonstrated relatively good scalability and fault tolerance of the method proposed in this paper.

Data Availability

The data used to support the findings of this study are available from the corresponding author upon request.

Conflicts of Interest

The authors declare no conflicts of interest.

Acknowledgments

This research study is sponsored by NSFC (61973314) Xi'an Science and Technology Project, (YJG 2020KJRC0132), Science and Technology Plan Projects in Shaanxi Province, (2021KRM025, 2021JM-537, and 2021GY-341). The authors thank these projects for supporting this article!

References

[1] J. Chen, S. Song, and H. Yu, "An indoor multi-source fusion positioning approach based on pdr/mm/wifi," *AEU - International Journal of Electronics and Communications*, vol. 135, no. 1, p. 153733, 2021.

[2] Z. Yuan, X. Zha, and X. Zhang, "Adaptive multi-type fingerprint indoor location and localization method based on multi-task learning and weight coefficients k-nearest neighbor," *Sensors*, vol. 20, no. 18, pp. 174–183, 2020.

[3] X. Chen, Q. Chen, and W. Wei, "An indoor location scheme for visible light using fingerprint database with multi.parameters," *ZTE Communications*, vol. 15, no. 1, pp. 43–48, 2017.

[4] H. Tang, F. Xue, T. Liu, M. Zhao, and C. Dong, "Indoor positioning algorithm fusing multi-source information," *Wireless Personal Communications*, vol. 109, no. 4, pp. 2541–2560, 2019.

[5] C. H. Cheng, Y. H. Kuo, and Z. Zhou, "Tracking nosocomial diseases at individual level with a real-time indoor location system," *Journal of Medical Systems*, vol. 42, no. 11, pp. 1–21, 2018.

[6] M. Zhou, X. Li, Y. Wang, S. Li, and W. Nie, "6g multi-source information fusion based indoor location via Gaussian kernel density estimation," *IEEE Internet of Things Journal*, vol. 13, no. 9, pp. 2753–2756, 2020.

[7] Z. Zhu, Y. Wang, and W. Liu, "Research on indoor location algorithm for multi-distance fusion," *Electronic Science and Technology*, vol. 206, no. 9, p. 26, 2019.

[8] H. Zhao, W. Cheng, N. Yang, S. Qiu, Z. Wang, and J. Wang, "Smartphone-based 3d indoor pedestrian positioning through multi-modal data fusion," *Sensors*, vol. 19, no. 20, p. 4554, 2019.

[9] M. Arnold, J. Hoydis, and S. T. Brink, "Novel massive mimo channel sounding data," *Applied to Deep Learning-Based Indoor Location*, vol. 36, no. 2, pp. 22–33, 2018.

[10] X. Wang, Y. Liu, H. Zhang, Q. Ma, and Z. Cao, "Public health emergency management and multi-source data technology in China," *Intelligent Automation & Soft Computing*, vol. 191, no. 15, pp. 493–508, 2018.

[11] X. Li, Z. Yan, L. Huang, S. Chen, and M. Liu, "High-accuracy and real-time indoor location system based on visible light communication and mobile robot," *International Journal of Optics*, vol. 2020, Article ID 3124970, 11 pages, 2020.

[12] L. Fernandes, S. Santos, M. Barandas, D. Folgado, and H. Gamboa, "An infrastructure-free magnetic-based indoor location system with deep learning," *Sensors*, vol. 13, no. 3, pp. 744–746, 2020.

[13] O. Hashem, K. A. Harras, and M. Youssef, "Accurate indoor location using ieee 802.11mc round trip time," *Pervasive and Mobile Computing*, vol. 18, no. 8, pp. 1816–1830, 2021.

[14] Y. T. Liu, R. Z. Sun, X. N. Zhang, L. Li, and G. Q. Shi, "An autonomous positioning method for fire robots with multi-source sensors," *Wireless Networks*, vol. 12, no. 21, pp. 200–203, 2021.

[15] E. Hu, Z. Deng, Q. Xu, L. Yin, and W. Liu, "Relative entropy-based kalman filter for seamless indoor/outdoor multi-source fusion positioning with ins/tc-ofdm/gnss," *Cluster Computing*, vol. 22, no. S4, pp. 8351–8361, 2018.